Article ID: 1003－6326(2003)01－0033－05

Electrochemical properties of TiV-based hydrogen storage alloys①

ZHU Yun-feng(朱云峰), LI Rui(李 锐), GAO Ming-xia(高明霞),
LIU Yong-feng(刘永锋), PAN Hong-ge(潘洪革), WANG Qi-dong(王启东)
(Department of Materials Science and Engineering, Zhejiang University, Hangzhou 310027, China)

Abstract: The electrochemical properties of the super-stoichiometric TiV-based hydrogen storage electrode alloys $(Ti_{0.8}Zr_{0.2})(V_{0.533}Mn_{0.107}Cr_{0.16}Ni_{0.2})_x$ (x = 2, 3, 4, 5, 6) were studied. It is found by XRD analysis that all the alloys mainly consist of a C14 Laves phase with hexagonal structure and a V-based solid solution phase with BCC structure. The lattice parameters and the unit cell volumes of the two phases decrease with increasing x. The cycle life, the linear polarization, the anode polarization and the electrochemical impedance spectra of the alloy electrodes were investigated systematically. The overall electrochemical properties of the alloy electrode are found improved greatly as the result of super-stoichiometry and get to the best when x = 5.

Key words: super-stoichiometry; TiV-based hydrogen storage alloy; C14 Laves phase; V-based solid solution; electrochemical property

CLC number: TG 139 **Document code:** A

1 INTRODUCTION

Nickel-metal hydride (Ni-MH) secondary batteries using hydrogen storage alloys as negative electrode materials have been widely studied and developed for their higher capacity, higher high-rate dischargeability (HRD), better cycling property and improved environmental compatibility compared with the Ni-Cd batteries[1-4]. Up to now, several series of hydrogen storage alloys have been studied, for example, the rare earth-based AB_5 type alloys[5], the Ti, Zr-based or Zr, Ti-based AB_2 type alloys[6,7], the Mg-based alloys[8] and the V-based alloys[9]. However, each of the alloy series has its potential problems, for instance, the comparatively low discharge capacity of the AB_5 type alloys, the poor cycling stability of the Mg-based alloys and the V-based alloys and the low HRD of the Ti- or Zr-based AB_2 type alloys. It is considered that the non-stoichiometry is an effective technique for improving the electrochemical properties of the hydrogen storage alloys. Lee et al[10] formulated a kind of hypo-stoichiometric Zr-based hydrogen storage alloys, which appeared very promising. The cycle life was found improved by over-stoichiometry. Notten et al[11] and Vogt et al[12] discovered that the $La(Ni, Cu)_{5+x}$ electrodes and $La(Ni, Sn)_{5+x}$ electrodes show a better cycling durability than the stoichiometric ones do. Based on the results of these investigations, we believe that the non-stoichiometry technique is an effective way to improve the overall electrochemical properties of the hydrogen storage alloys to be studied.

The TiV-based AB_2 type Ti-Zr-V-Mn-Cr-Ni hydrogen storage alloy was selected for it generally has a higher discharge capacity than the rare earth-based AB_5 type alloy. We formulated a super-stoichiometric hydrogen storage alloy series $(Ti_{0.8}Zr_{0.2})-(V_{0.533}Mn_{0.107}Cr_{0.16}Ni_{0.2})_x$ (x = 2, 3, 4, 5, 6) rather boldly and the electrochemical properties of these alloys were investigated systematically.

2 EXPERIMENTAL

The alloys $(Ti_{0.8}Zr_{0.2})(V_{0.533}Mn_{0.107}Cr_{0.16}Ni_{0.2})_x$ (x = 2, 3, 4, 5, 6) were prepared by induction levitation melting of the constituent metals in a water-cooled copper crucible under argon atmosphere. The ingots were turned over and remelted twice for homogeneity. Part of the alloys were mechanically crushed and ground into powders with diameter size < 47 μm for XRD and electrochemical measurements.

Crystal structures and lattice parameters of the alloys were determined by X-ray diffraction (XRD) on a Philips diffractometer with CuK_α radiation. All test electrodes were prepared by mixing 0.1 g alloy powder with 0.4 g carbonyl nickel powder and then cold-pressing the mixture under a pressure of 25 MPa into a pellet with the diameter of 10 mm and thickness of about 1 mm. The electrochemical measurements were performed in a half-cell consisting of a working electrode (MH electrode), a sintered $Ni(OH)_2$/NiOOH counter electrode and an Hg/HgO reference electrode. The electrolyte was a 6 mol/L KOH solution, controlled at (30±1) ℃. In order to reduce the IR

① **Received date:** 2002－03－17; **Accepted date:** 2002－06－16

Correspondence: PAN Hong-ge, Professor of Department of Materials Science and Engineering, Zhejiang University, Hangzhou 310027, China, Tel: +86-571-87952576, Fax: +86-571-87951152, E-mail: pan_hg@mail.hz.zj.cn

drop, the Hg/HgO reference electrode was equipped with a Luggin tube. The discharge capacity of the electrode was determined by the galvanostatic method. Each electrode was charged at 100 mA/g for 5 h followed by 10 min rest and then discharged at 60 mA/g to the cut-off potential of − 0.6 V vs the Hg/HgO reference electrode. Electrochemical impedance spectroscopy (EIS) measurements were conducted at 50% depth of discharge (DOD) using Solartron SI1287 Electrochemical Interface with a 1255B Frequency Response Analyzer, using the ZPLOT electrochemical impedance software. Before EIS measurements, the test electrodes were completely activated (15 cycles). The EIS of the electrodes were obtained in the frequency range of 100 kHz to 5 mHz with an AC amplitude of 5 mV under open-circuit conditions. The linear polarization curves and the anode polarization curves of the test electrodes were measured by scanning the electrode potentials (Solartron SI1287 potentionstat, using the CorrWare electrochemistry/corrosion software) at the rate of 0.1 mV/s from − 5 mV to 5 mV (vs. open circuit potential) and 5 mV/s from 0 to 1 200 mV (vs open circuit potential) at 50% depth of discharge (DOD), respectively.

3 RESULTS AND DISCUSSION

3.1 Alloy structures

Fig. 1 shows the XRD patterns of $(Ti_{0.8}Zr_{0.2})(V_{0.533}Mn_{0.107}Cr_{0.16}Ni_{0.2})_x$ (x = 2, 3, 4, 5, 6) alloys. It can be seen that all the alloys are mainly composed of a C14 Laves phase with hexagonal structure and a V-based solid solution phase with BCC structure. The lattice parameters of the two phases are listed in Table 1. As listed in Table 1, when x increases, the lattice parameters and the unit cell volumes of both phases all decrease. From

Table 1 Characteristics of alloy phases in $(Ti_{0.8}Zr_{0.2})(V_{0.533}Mn_{0.107}Cr_{0.16}Ni_{0.2})_x$ (x = 2, 3, 4, 5, 6) alloys

Sample	Phase	Lattice parameter/ 10^{-10} m		Cell volume/ 10^{-30} m^3
	C14	a = 5.023	c = 8.190	179.00
x = 2	BCC	a = 3.012		27.33
	C14	a = 4.967	c = 8.105	173.20
x = 3	BCC	a = 2.986		26.62
	C14	a = 4.937	c = 8.057	170.10
x = 4	BCC	a = 2.977		26.38
	C14	a = 4.920	c = 8.017	168.10
x = 5	BCC	a = 2.973		26.28
	C14	a = 4.897	c = 7.983	165.80
x = 6	BCC	a = 2.962		25.99

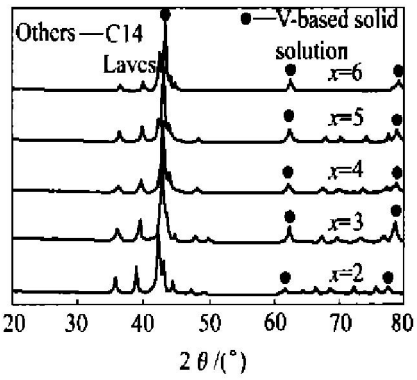

Fig. 1 XRD patterns of $(Ti_{0.8}Zr_{0.2})(V_{0.533}Mn_{0.107}Cr_{0.16}Ni_{0.2})_x$ (x = 2, 3, 4, 5, 6) alloy eletrodes

the patterns, it can also be seen that the peak intensity of the C14 Laves phase becomes weaker, which makes us believe that the content of the C14 Laves phase decreases while the V-based solid solution phase content increases in the alloys with higher stoichiometry.

3.2 Electrochemical characteristics

3.2.1 Discharge behavior and cycle life

Fig. 2 shows the variation of the discharge midpoint potentials and the open circuit potentials at 50% DOD (depth of discharge) of the alloy electrodes. It is obvious that both potentials increase with increasing x. However, the difference between the two potentials decreases, which indicates that the discharge overpotential and the polarization of the alloy electrode decrease with higher stoichiometry.

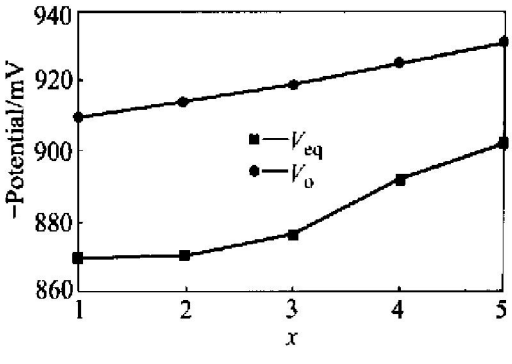

Fig. 2 Variation of discharge midpoint potentials V_{eq} and open circuit potentials V_o of $(Ti_{0.8}Zr_{0.2})(V_{0.533}Mn_{0.107}Cr_{0.16}Ni_{0.2})_x$ (x = 2, 3, 4, 5, 6) alloy electrodes at 50% DOD and 303 K

Fig. 3 shows the maximum discharge capacities of the $(Ti_{0.8}Zr_{0.2})(V_{0.533}Mn_{0.107}Cr_{0.16}Ni_{0.2})_x$ (x = 2, 3, 4, 5, 6) alloy electrodes. It can be seen that the maximum discharge capacity increases when x increases from 2 to 5. Tsukahara et al[13] reported that the

single V-based solid solution phase had very little electrochemical discharge capacity in the KOH electrolyte because it has no electrocatalytic activity. But with the presence of other phases in the V-based alloys such as TiNi phase, which acted as a catalyst and a micro-current collector, the V-based solid solution phase was activated to absorb and desorb reversibly a considerable amount of hydrogen in KOH electrolyte. In the present work, the alloys are all mainly composed of two phases, of which both the C14 Laves phase and the V-based solid solution phase, especially, are the hydrogen storage phases, with the C14 Laves phase working as the catalyst and the micro-current collector. Therefore, the increase in maximum discharge capacity here may be ascribed to the increase in content of the V-based solid solution phase with increasing x as determined by XRD analysis. But when x reaches 6, the maximum discharge capacity decreases. We try to attribute this phenomenon to the competition between increasing V-based solid solution phase content and decreasing electrocatalytic activity of the C14 Laves phase. It has been concluded that the V-based solid solution phase content increases, while the C14 Laves phase content decreases all the time with increasing x. Since the C14 Laves phase works as a catalyst and a micro-current collector, the decrease in C14 Laves phase content will lead to the decrease in electrochemical activity of the V-based solid solution phase. Consequently, we believe that it is natural for this type of electrode to have a maximum discharge capacity and subsequently decline in capacity with increasing x. In this study, the discharge capacity of the alloy electrode reaches the maximum of 379.8 mA·h/g when x = 5 and then decreased to 320.3 mA·h/g when x = 6.

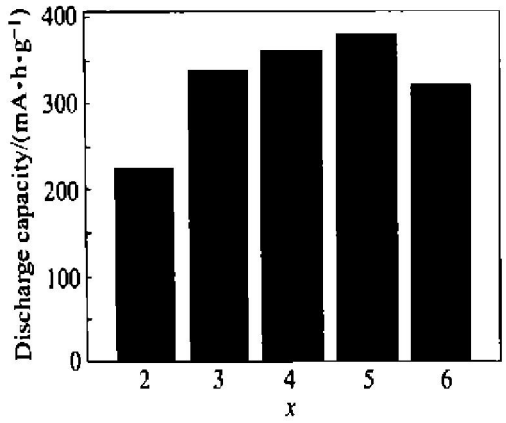

Fig. 3 Maximum discharge capacities of $(Ti_{0.8}Zr_{0.2})(V_{0.533}Mn_{0.107}Cr_{0.16}Ni_{0.2})_x$ (x = 2, 3, 4, 5, 6) alloy electrodes

Fig. 4 shows the activation cycles and the discharge capacity retention of the 100 th cycle (C_{100}/C_{max}) of $(Ti_{0.8}Zr_{0.2})(V_{0.533}Mn_{0.107}Cr_{0.16}Ni_{0.2})_x$ (x = 2, 3, 4, 5, 6) alloy electrodes. It can be seen that the cycling stability of the alloy electrode is improved, while the activation property is worsened with increasing x. For x = 6, the discharge capacity of the electrode still remains 85.79% of the maximum discharge capacity even after 100 charge-discharge cycles, while it needs 15 cycles to activate the electrode. It has been reported that Cr element is very favorable for the cycling durability of the Ti-based alloy electrode due to its corrosion-resistant capability in the alkaline electrolyte by forming a passive oxide film on the electrode surface, which retards the oxidation and dissolution of other elements[14]. We also believe that the increase of Cr content in the alloy due to the increase of B side stoichiometry here is responsible for the increasing cycling stability of the alloy electrode. On the other hand, the passive film at the same time lowers the activation property and makes the electrode more difficult to be activated.

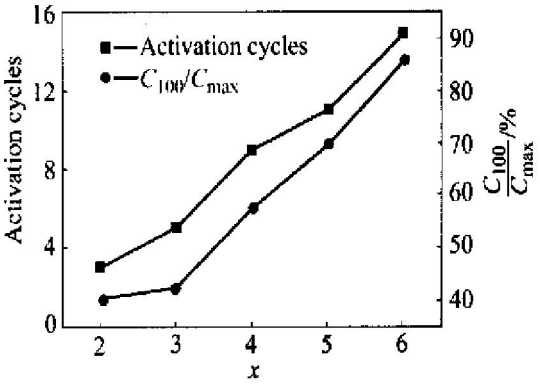

Fig. 4 Activation cycles and discharge capacity retention of 100 th cycle(C_{100}/C_{max}) of $(Ti_{0.8}Zr_{0.2})(V_{0.533}Mn_{0.107}Cr_{0.16}Ni_{0.2})_x$ (x = 2, 3, 4, 5, 6) alloy electrodes

3.2.2 Electrochemical kinetics

The exchange current density J_0 calculated from the linear polarization of the $(Ti_{0.8}Zr_{0.2})$-$(V_{0.533}Mn_{0.107}Cr_{0.16}Ni_{0.2})_x$ (x = 2, 3, 4, 5, 6) alloy electrodes are listed in Table 2. It can be found that J_0 increased from 64.4 mA/g(x = 2) to 161.4 mA/g(x = 5) and then decreased to 148.8 mA/g when x = 6.

Table 2 Exchange current density J_0 and limiting current density J_L of $(Ti_{0.8}Zr_{0.2})(V_{0.533}Mn_{0.107}Cr_{0.16}Ni_{0.2})_x$ (x = 2, 3, 4, 5, 6) alloy electrodes

Sample	Linear polarization, J_0/(mA·g^{-1})	AC impedance, J_0/(mA·g^{-1})	J_L/(mA·g^{-1})
x = 2	64.4	44.1	509.4
x = 3	121.5	88.6	999.2
x = 4	125.1	106.9	1 065.9
x = 5	161.4	142.5	1 608.3
x = 6	148.8	128.2	1 548.8

The limiting current density J_L, which is obtained from the anode polarization of the $(Ti_{0.8}Zr_{0.2})(V_{0.533}Mn_{0.107}Cr_{0.16}Ni_{0.2})_x$ (x= 2, 3, 4, 5, 6) alloy electrodes are also listed in Table 2, it can be found that J_L is increased from 509.4 mA/g(x= 2) to 1 608.3 mA/g(x= 5) and then decreased to 1 548.8 mA/g when x= 6. The variation is consistent with that of the exchange current density J_0.

Fig. 5 shows the electrochemical impedance spectra of the $(Ti_{0.8}Zr_{0.2})(V_{0.533}Mn_{0.107}Cr_{0.16}Ni_{0.2})_x$ (x= 2, 3, 4, 5, 6) alloy electrodes at 50% DOD. It can be seen that, for all the alloys, the EIS consist of two semicircles followed by a straight line at low frequency. According to the analysis model proposed by Kuriyama et al[15], an equivalent circuit adopted for the metal hydride electrode is also shown in Fig. 6. The constant-phase elements (CPE), $Q_i(\omega)=\{Y_{0i}(j\omega)^n\}^{-1}(0<n<1)$, are applied for the capacitive components to describe the depressed shape of the semicircles[16]. R_1 is the solution resistance between the alloy electrode and the reference electrode. The semicircle in the high-frequency region results from R_2 and Q_2 is ascribed to the contact resistance between the electrode pellet and the current collector. R_3 and C_3 are responsible for the contact resistance between the alloy powder and the nickel powder in the electrode pellet. The semicircle in the low-frequency region, characterized by R_4 and Q_4, is attributed to the charge-transfer resistance and the double-layer capacitance, respectively. W_4 is the Warburg impedance corresponds to the hydrogen diffusion in the alloy. It can be found from Fig. 5 that the radius of the larger semicircle in the low frequency region decreases with increasing x from 2 to 5, and then slightly increases when x= 6, which indicates that the charge-transfer resistance of the electrode surface is decreased to a minimum from x= 2 to 5 and then increased when x reaches 6. The parameters in the equivalent circuit were fitted using the ZPLOT electrochemical impedance software. The exchange current density J_0 calculated from the charge-transfer resistance(listed in Table 2) is found to increase from 44.1 mA/g(x= 2) to 142.5 mA/g(x= 5) and then decrease to 128.2 mA/g when x = 6. The variation is consistent with that of the linear polarization.

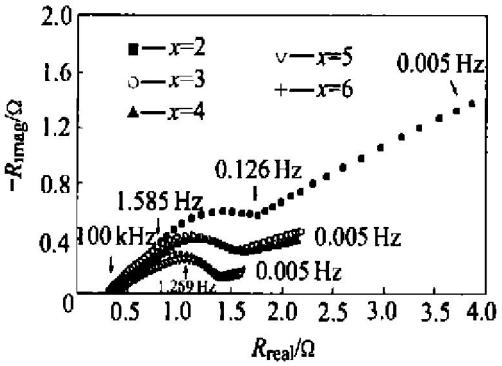

Fig. 5 Electrochemical impedance spectra of $(Ti_{0.8}Zr_{0.2})(V_{0.533}Mn_{0.107}Cr_{0.16}Ni_{0.2})_x$ (x= 2, 3, 4, 5, 6) alloy electrodes measured at 50% depth of discharge(DOD) and 298 K

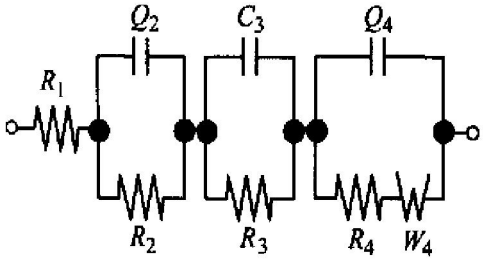

Fig. 6 Equivalent circuit for $(Ti_{0.8}Zr_{0.2})$-$(V_{0.533}Mn_{0.107}Cr_{0.16}Ni_{0.2})_x$ (x= 2, 3, 4, 5, 6) metal hydride electrodes

From above results, it is believed that the kinetics of hydriding of the super-stoichiometric $(Ti_{0.8}Zr_{0.2})(V_{0.533}Mn_{0.107}Cr_{0.16}Ni_{0.2})_x$ (x= 2, 3, 4, 5, 6) hydrogen storage alloys is greatly improved with increasing x, and the optimal composition was found to lie in x= 5.

4 CONCLUSION

The results show that the TiV-based hydrogen storage alloys all mainly consist of a C14 Laves phase with hexagonal structure and a V-based solid solution phase with BCC structure. The C14 Laves phase content decreases and the V-based solid solution phase content increases with increasing x. Electrochemical measurements show that the maximum discharge capacity, the discharge equilibrium potential, the cycling stability, the exchange current density J_0 and the limiting current density J_L of the alloy electrode all increase with increasing x from 2 to 5. When x reaches 6, the discharge equilibrium potential and the cycling stability still increase proportionately, while the maximum discharge capacity, the exchange current density J_0 and the limiting current density J_L are decreased. Furthermore, the discharge overpotential decreases with increasing x and the alloy electrode becomes more difficult to be activated for higher stoichiometry. After considering the global effect of the non-stoichiometry of B side on the performances of the alloy electrodes, it can be concluded that the optimal composition lies in x= 5.

REFERENCES

[1] Willems J J G. Metal hydride electrodes stability of $LaNi_5$-related compounds[J]. Philips J Res Suppl 1984, 39(1): 1.

[2] Sakai T, Miyamura H, Kuriyama N, et al. Metal hydride anodes for nickel-hydrogen secondary battery[J]. J Electrochem Soc, 1990, 137: 795-799.

[3] PAN Hong-ge, CHEN Yun, WANG Churn-sheng, et al. Ef-

fect of alloys modified by an alkaline solution containing potassium borohydride on the kinetic properties of $MlNi_{3.7}Co_{0.6}Mn_{0.4}Al_{0.3}$ hydride electrode[J]. Electrochim Acta, 1999, 44: 2263 - 2269.

[4] Wang C S, Lei Y Q, Wang Q D. Studies of electrochemical properties of TiNi alloy used as an MH electrode-Ⅰ[J]. Discharge capacity Electrochim Acta, 1998, 43: 3193 - 3207.

[5] Pan H G, Ma J X, Wang C S, et al. Effect of Co content on the kinetic properties of the $MlNi_{4.3-x}Co_xAl_{0.7}$ hydride electrodes[J]. Electrochim Acta, 1999, 44: 3977 - 3987.

[6] Yu J S, Lee S M, Cho K, et al. The cycle life of $Ti_{0.8}Zr_{0.2}V_{0.5}Mn_{0.5-x}Cr_xNi_{0.8}$ (x = 0 to 0.5) alloys for metal hydride electrodes of Ni-metal hydride rechargeable battery[J]. J Electrochem Soc, 2000, 147(6): 2013 - 2017.

[7] Kim D M, Lee S M, Jang K J, et al. The electrode characteristics of over-stoichiometric $ZrMn_{0.5}V_{0.5}Ni_{1.4+y}$ (y = 0.0, 0.2, 0.4 and 0.6) alloys with C15 Laves phase structure [J]. J Alloys Comp, 1998, 268: 241 - 247.

[8] Iwakura C, Inoue H, Zhang S G, et al. Raman and X-ray photoelectron spectroscopic investigations on a new electrode material for nickel-metal hydride batteries: MgNi-graphite composites prepared by ball-milling[J]. J Electrochem Soc, 1999, 146(5): 1659 - 1663.

[9] Tsukahara M, Kamiya T, Takahashi K, et al. Hydrogen storage and electrode properties of V-based solid solution type alloys prepared by a thermic process[J]. J Electrochem Soc, 2000, 147(8): 2941 - 2944.

[10] Lee S M, Kim S H, Jeon S W, et al. Study on the electrode characteristics of hypostoichiometric Zr-Ti-V-Mn-Ni hydrogen storage alloys[J]. J Electrochem Soc, 2000, 147 (12): 4464 - 4469.

[11] Notten P H L, Einerhand R E F, Daams J L C. On the nature of the electrochemical cycling stability of non-stoichiometric $LaNi_5$-based hydride-forming compounds Part Ⅰ — crystallography and electrochemistry[J]. J Alloys Comp, 1994, 210: 221 - 232.

[12] Vogt T, Reilly J J, Johnson J R, et al. Crystal structure of nonstoichiometric $La(Ni, Sn)_{5+x}$ alloys and their properties as metal hydride electrodes[J]. Electrochem Solid-State Lett, 1999, 2(3): 111 - 114.

[13] Tsukahara M, Takahashi K, Mishima T, et al. Vanadium-based solid solution alloys with three-dimensional network structure for high capacity metal hydride electrodes[J]. J Alloys Comp, 1997, 253 - 254: 583 - 586.

[14] Yu J S, Liu B H, Cho K, et al. The effects of partial substitution of Mn by Cr on the electrochemical cycle life of Ti-Zr-V-Mn-Ni alloy electrodes of a Ni/MH battery[J]. J Alloys Comp, 1998, 278: 283 - 290.

[15] Kuriyama N, Sakai T, Miyamura H, et al. Electrochemical impedance and deterioration behavior of metal hydride electrodes[J]. J Alloys Comp, 1993, 202: 183 - 197.

[16] Boukamp B A. A nonlinear least squares fit procedure for analysis of impedance data of electrochemical systems[J]. Solid State Ionics, 1986, 20: 31.

(Edited by HUANG Jin-song)